HERA-19 Commissioning: More Results from Sky Calibration
HERA Memorandum Number 32
July 2017

C.L. Carilli[1,2], B. Nikolic[2], K. Gale-Sides[2], G. Bernardi[3]

ccarilli@aoc.nrao.edu

ABSTRACT

We present further results from sky calibration, comparing Galactic Center (GC) calibration, to independent calibration using two sources at 21hr (the 'Bernardi Sources', BS). Full calibration can be performed using the BS sources (delays, mean phase, bandpass), resulting in reasonable images, although with lower signal to noise relative to the Galactic center. The delay solutions match well between GC and BS calibration. However, the bandpass solutions do not match. The latter result suggests that the bandpass solutions reflect some combination of the true antenna response as a function of frequency, coupled with calibration model limitations, and possibly other antenna-specific responses. We find that bandpass amplitude solutions are strongly influenced by the data on the shortest baselines, where the signal to noise is highest, ie. the bandpass amplitude solutions change substantially when the shortest baselines are left out of the calibration process. Interestingly, the phase solutions appear to be more robust to using different baselines in the calibration. We see evidence for a sinusoidal pattern in both the bandpass solutions, and in some of the visibilities on certain short spacings, for the GC data. The wavelength is about 20MHz across the bandpass spectrum, corresponding to 15m of pathlength, if it was a standing wave. We investigate whether this pattern could be a standing wave within the structure of the dish itself, or a resonance between antennas in a baseline, or again, missing structure in the calibration model. The characteristic scale of 15m is close to the round trip distance from the feed to the edge of the dish, or the near-edge of neighboring antennas, hence suggestive of a standing wave.

[1]National Radio Astronomy Observatory, P. O. Box 0, Socorro, NM 87801

[2]Cavendish laboratory, Cambridge University, UK

[3]SKA-SA Project Office, Capetown, & Rhodes University, South Africa

However, there are other characteristics that argue for missing structure in the input calibration model. We will continue to investigate this type of spectral behaviour. On a positive note, even if this is a standing wave or resonance between antennas on short baselines, the wavelength is long, as predicated in the original HERA design, and hence may not couple strongly into a delay power-spectral analysis.

1. Data and Processing

This is the fourth in a series of memos analyzing HERA-19 data from 2016. We again analyze data from June 2016 for the HERA-19 array. For completeness, we repeat the basic info on the data and processing, from Nikolic et al. (2016), as follows:

The array and data format (bandwidth, channel width, time resolution), are desribed in Carilli (2016). The data were converted to CASA measurement sets using processes described in Nikolic et al. (2016). Flagging by channel was applied based on visual inspection of visibility spectra, and known bad antennas were flagged, leaving 17 antennas total.

The sky calibration process is described in detail in Nikolic et al. (2016). In brief, after flagging, the antenna based delays are derived using the 'K' solution option in gaincal in CASA, and using a point source model for the GC. This process removes the significant phase slopes as a function of frequency seen in the measured visibilities, effectively removing any phase wraps over the band. A second gaincal is then run to determine the mean phase offset across the band for each antenna.

The resulting data set is then imaged with CLEAN to produce a CLEAN component model of the extended emission across the GC. This CLEAN model is than used to determine the complex bandpasses of the antennas (amplitude and phase versus frequency). A second iteration is performed, leading to the final bandpasses.

We then apply the resulting calibration (delays, mean phase offsets, bandpasses) to the data, and to data taken at other times of day.

2. Results

2.1. Calibrating with the Bernardi Sources

In this memo, we consider in more detail the two 'Bernardi sources' (BS) at 21hr: J2107-2519 with a flux density of 34Jy at 150MHz, and J2101-2802 with a flux density of 22Jy at 150MHz (flux densities from G. Bernardi).

We perform two independent calibration procedures. First, we perform all the calibration on the Galactic Center, and apply the delay, mean phase, and bandpass solutions to the Bernardi source data, and image. Second, we start from the raw data on the Bernardi sources, and perform the full calibration using a two point source model for the field. We start from delays and go through the full imaging and bandpass selfcalibration process. We then compare the results in the calibration solutions, the visibility spectra, and the final images.

We start by showing the final images from the two processes, for reference. The two source are clear in each, which is encouraging. The positions and flux densities (in arbitrary units), from the GC calibration are: 21:07:34.9 -25:16:49, with 0.036units, and 21:01:14.8 -28:05:49.5, with 0.030units. The positions and flux densities from the BS calibration are: 21:06:36.3 -25:19:35, with 0.05units, and 21:00:39.3 -28:10:23, with 0.05units. Note that the synthesized beam has FWHM = 1.4deg, so the position differences are very small with respect to the resolution.

Figure 2 shows the resulting delays from the GC calibration and the BS calibration. For most of the antennas, the solutions are similar, to within 5nsec or so. However, two antennas, antenna 73 and 81, have very different delay solutions from the GC process vs. the BS process.

The first attempt at the delay and bandpass solution using the BS sources themselves, resulted in the bandpass phase solutions vs. frequency for each antenna that is shown in Fig. 3. Clearly, the delay solutions for two antennas (again, 73 and 81), were incorrect. The bandpass calibration has attempted to compenstate for the erroneous delay solutions, resulting in the rapid wrapping of the phase vs. frequency caused by applying the wrong delay. These large delay errors for the two antennas also affected the bandpass solutions for the other antennas. This is a beautiful example of what happens in subsequent calibration if the original delays are incorrect by a large factor. We believe that the delay solutions for these two antennas failed due to low signal-to-noise. We then flagged these two antennas, and restarted the calibration process from scratch.

Figure 4 shows the final phase and amplitude bandpass solutions for both the GC and

and BS calibrations. The bandpass solutions are different from the two processes. Unless the system response has changed dramatically between the two observing times[1], these large differences are likely attributed to insufficient information in the input calibration models, ie. the calibration is compensating for model errors through corrections to the bandpass.

Figure 5 shows the resulting visibility spectra of the BS souces, from the BS and GC calibration, respectively, for all baselines to antenna 32. Interestingly, even though the bandpasses solutions look markedly different, the visibility spectra show a general agreement in overall shape for most baselines, including eg. some of the smaller scale structure in the phase vs. frequency. Of course, the corresponds is far from exact, eg. there appears to be a systematic phase offset, but apparently the calibrated visibility spectra are close enough to produce images showing the two sources (Fig 1).

The final GC calibrated image looks 'better' than the BS calibrated image, in terms of what one might consider imaging artefacts and related, although this is difficult to confirm, given we don't really know what the field should look like. Formally, the off-source rms in the GC image is a factor 2 lower than the BS image.

Given a source flux density, we can estimate the noise in the image, and compare that to what we might expect theoretically. Using J2101-2802, the flux of the source is 22Jy at 150MHz. The source has a measured flux density of 0.034units on the image. The rms noise on the image is 0.0004units. Taking the ratios, and scaling by the source flux density, the implied noise is then 0.24 Jy beam^{-1}. Using 17 antennas, 14m diameter, 70% efficiency, 50MHz bandwidth, 10min integration, and T_{sys} = 500K, the expected rms noise is 4.4mJy. This result implies that the image is not noise limited, but severely limited by dynamic range and/or confusion.

Overall, it appears both calibration methods get us to a final image with two sources, as expected, although it is also clear that the bandpass solutions are compensating for inadequancies in the models. Currently, the GC calibration has higher S/N, and hence appears to be more effective. This will change as the array grows. We believe as more antennas, and longer baselines, are employed, the models will improve, and we are hopeful that the process will converge to correct antenna-based calibration responses vs. frequency, and higher dynamic range images.

---

[1]Note that in HERA memo. 23 we concluded that the system response is relatively stable over daily timescales

2.2. Resonances and Ripples

We are interested in investigating the possibility of electromagnetic cross coupling or other resonances in HERA elements, such as standing wave within the structure of a given antenna, or resonances between two antennas, or other phenomena one might expect for a close packed array. Note that all the data analyzed in this section correspond to the Galactic Center.

Figure 6 and 7, we show a series of spectra for two antennas (10 and 11). The plots include: (i) the bandpass solution for an antenna from the GC calibration, (ii) autocorrelation spectra with and without the bandpass applied, and (iii) cross correlation spectra with and without bandpass calibration.

We start with antenna 11, which is a relatively 'good' antenna. The resulting calibrated cross and auto correlation spectra look fairly smooth. The only anomaly is a 3% hump in the bandpass around channel 470. This hump does not appear in the uncalibrated autocorrelation spectrum, and only appears in one short spacing in the cross correlations.

Antenna 10 (Fig 7) shows more curious behaviour. The resulting bandpass has a clear sinusoidal pattern, with a wavelength of about 20MHz across the bandpass spectrum, and an amplitude of about 10%. The implied pathlength for a reflection would be 15m for this sinusoid.

This pattern is not seen in the uncalibrated autocorrelation spectrum. Looking at the uncalibrated cross correlations to antenna 10, the sinusoidal pattern is seen clearly on two of the shortest baselines (the cyan and green curves at the top of figure). These correspond to baselines 10 to 106 (green) and 10 to 54 (green). Each of these is a 15m baselines, with an orientation 45° east of north. There is some indication of this pattern on another short baseline (10 to 21; black), which has a different orientation (east-west).

The fact that the bandpass resembles the raw visibility spectra on the shortest baselines suggests that the bandpass calibration is being heavily weighted to the short spacings. This result is not surprising, since the short baselines have the highest signal to noise. The important question is whether this spectral structure is the real response of the antenna, or some other resonance between antennas or within an antenna, or something else?

To investigate this question, Fig. 8 shows bandpass solutions for three antennas: 10 (blue), 73 (cyan), and 11 (green). The upper plots show the bandpass solutions using all baselines. The lower plots show the bandpass solutions leaving out the shortest baselines of the array (baselines shorter than 16m). For the amplitudes, the results are signicantly different. In particular, the sinusoidal pattern in the antenna 10 bandpass is gone when

omitting the short baselines from the bandpass calibration. The implication is that the resulting bandpasses are not reflecting the true antenna responses, since these should not change when using different baselines in the calibration. Interestingly, the phase solutions look similar with and without the short baselines in the bandpass calibration process.

Lastly, figure 9 shows uncalibrated visibility spectra for three baselines that have the same length and orientation: 10-106 (cyan), 23-73 (orange), and 105-54 (brown). The four-peak sinusoidal pattern is evident on all three baselines, although most prominent on 10-106.

What could cause this sinusoid in the raw visibility spectra, and the resulting bandpass?

Again, the wavelength across the spectrum is about 20MHz, implying 15m for a return-loss pathlength. The characteristic lengths scale in the system relative to feed are: focal height = 4.5m (or 9m round trip, or a 33MHz wavelength across the spectrum), distance to edge of disk = 7m (14m RT, 20MHz wavelength), and distance to next feed = 15m (30m RT or 10MHz wavelength). Hence, if this was a standing wave within an antenna itself, the wavelength of the standing wave corresponds to the roundtrip distance between the feed and the edge of the dish, or the edge of the neighboring dish. A standing wave between the feed and the center of the dish (hub), would lead to a broader ripple. On the other hand, the fact that the pattern only shows up on some baselines argues against a standing wave within the dish itself, which should manifest itself on all baselines to that antenna. Likewise, it does not show up in the autocorrelation, nor in the bandpass solutions from the Barnardi sources.

If this pattern was due to a coupling between two antenna feeds, then it could be baseline specific, but the wavelength would be 10MHz, not 20MHz.

If it was not a SW but missing structure in model, then it could indeed, be baseline length and orientation specific, but the 15m wavelength would then be fortuitous.

Perhaps the strongest argument against a standing wave or resonance is that the wavelength shifts with increasing frequency, with the peaks at the lower frequencies separated by about 15MHz, the peaks in the center separated by about 19MHz, and the peaks at the high end seperated by 23MHz.

Regardless of the cause, the wavelength is long with respect to the typical bandwidths that will be incorporated into the cosmological analysis (15m, as incorporated into the original HERA design), and hence may not couple strongly into a delay power-spectral analysis.

3. Thoughts

- We find that the bandpass solutions are reflecting some combination of the true antenna response as a function of frequency, coupled with calibration model limitations, and possibly other antenna-specific responses, such as standing waves between antennas.
- We can calibrate fully using the Bernardi sources, and obtain a two-source image, although signal to noise is a limitation for the HERA19 array.
- Bandpass solution amplitudes are strongly influenced by the data on the shortest baselines, where the signal to noise is highest. The amplitude solutions change substantially when a short baseline restriction is applied during the calibration process. Interestingly, the phase solutions appear to be robust to using different baselines in the calibration.
- We see evidence for sinusoidal structure in raw visibility spectra, and the resulting bandpass solutions, for the GC data, with a wavelength across the spectrum of about 20MHz (15m of pathlength for a reflection). Evidence currently disfavors a standing wave. We will continue to investigate this type of spectral behaviour.

References

Nikolic, B., Carilli, C., & Sims, P. 2016, HERA memo 22
(http://reionization.org/science/memos/)

Carilli, C. 2016, HERA memo 15
(http://reionization.org/science/memos/)

Carilli, C., & Sims, P. 2016, HERA memo 12
(http://reionization.org/science/memos/)

Carilli, C., Nikolic, B., & Gale-Sides, K. 2016, HERA memo 23
(http://reionization.org/science/memos/)

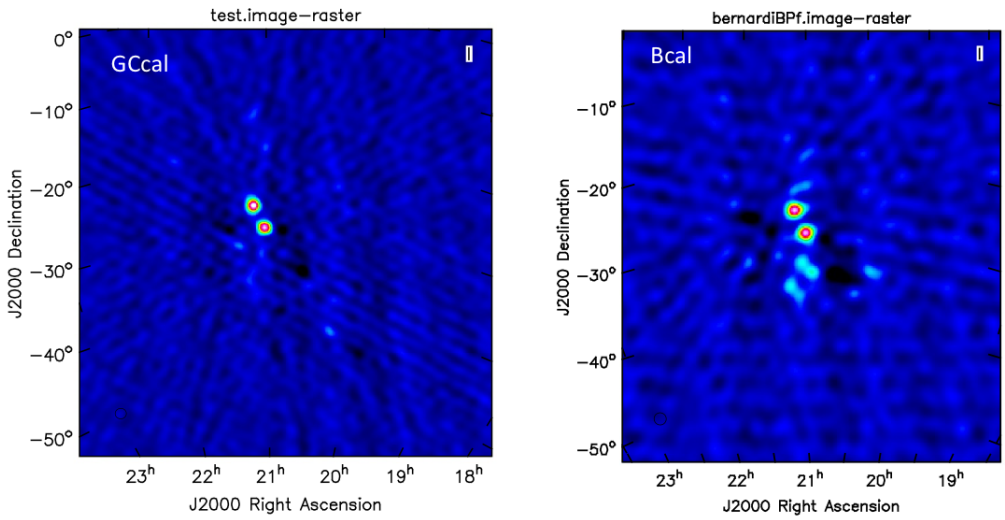

Fig. 1.— Left: Images of the Bernardi sources made using calibration derived on the Galatic Center. Right: Images of the Bernardi sources made using calibration derived on the sources themselves.

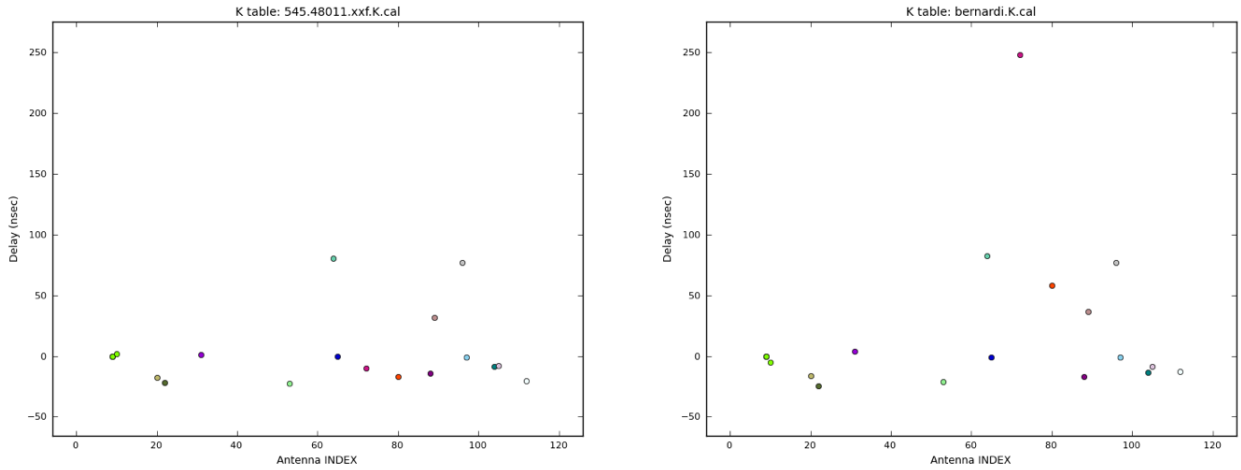

Fig. 2.— Left: Delay solutions vs. antenna number using the Galactic Center. Right: Delay solutions vs. antenna number, using the two Bernardi sources for calibration.

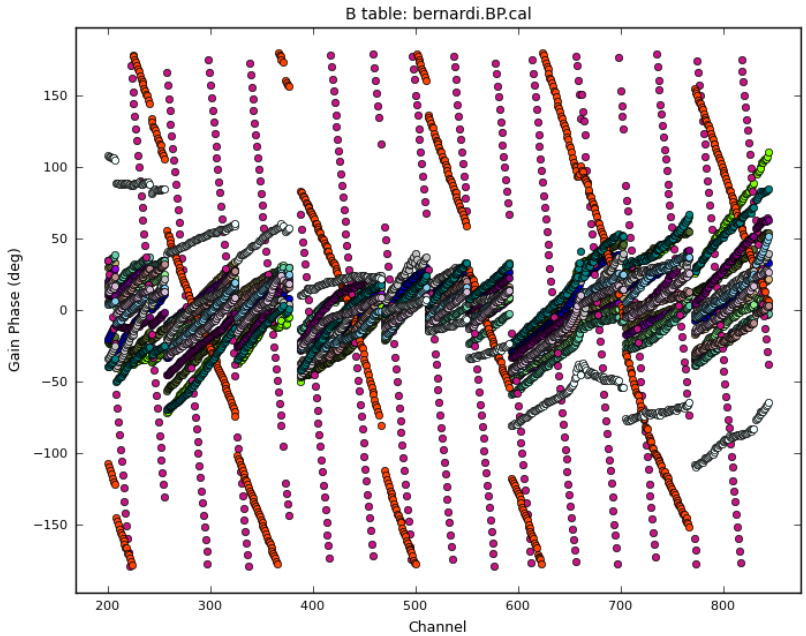

Fig. 3.— Bandpass solutions using the Bernardi sources for delay and bandpass calibration, and including the antennas 81 and 73, for which the delay solutions were likely bad.

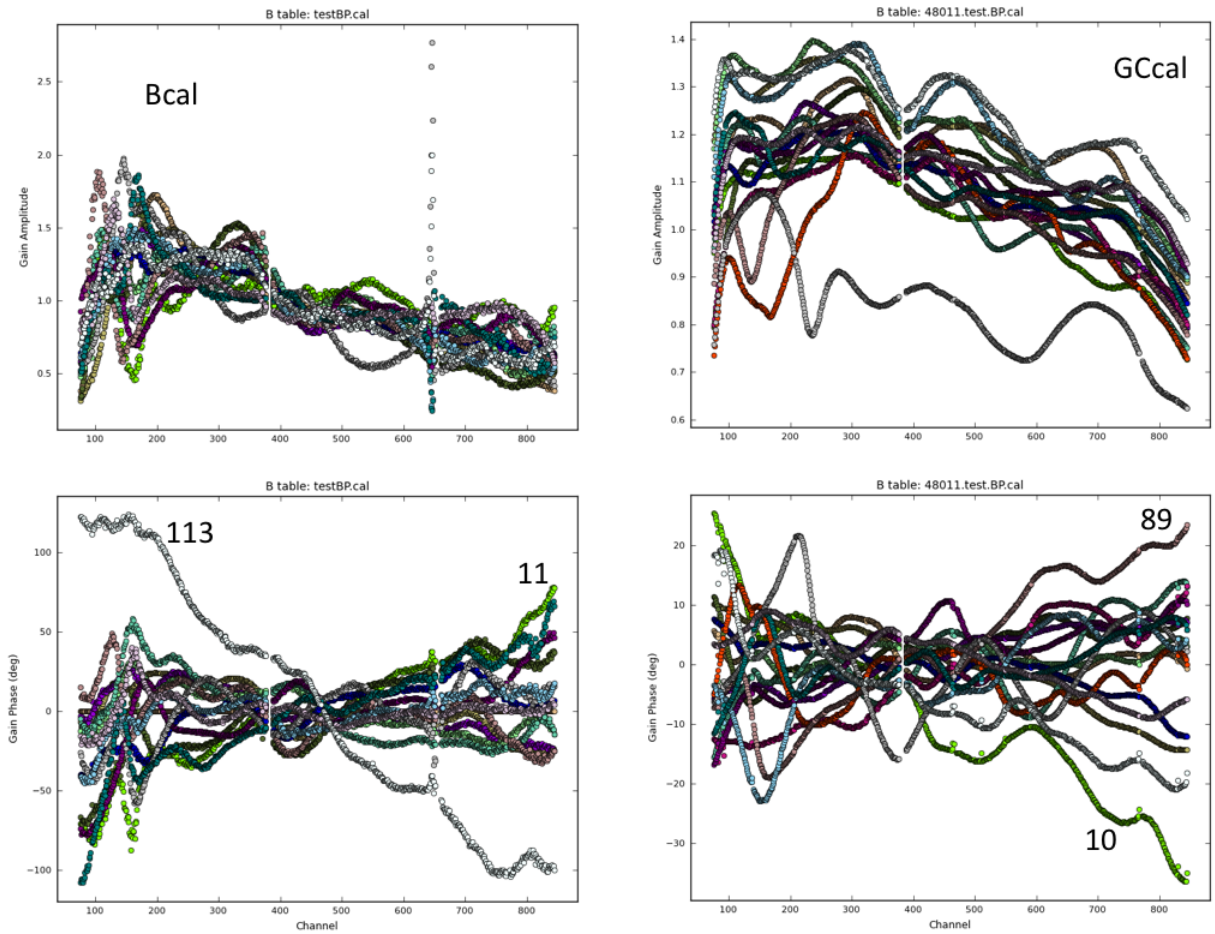

Fig. 4.— Left: Amplitude (top) and phase (bottom) bandpass solutions after flagging antennas 81 and 73, and using the Bernardi sources for delay and bandpass calibration. Right: Amplitude and phase bandpass solutions, and using the Galactic Center for delay and bandpass calibration.

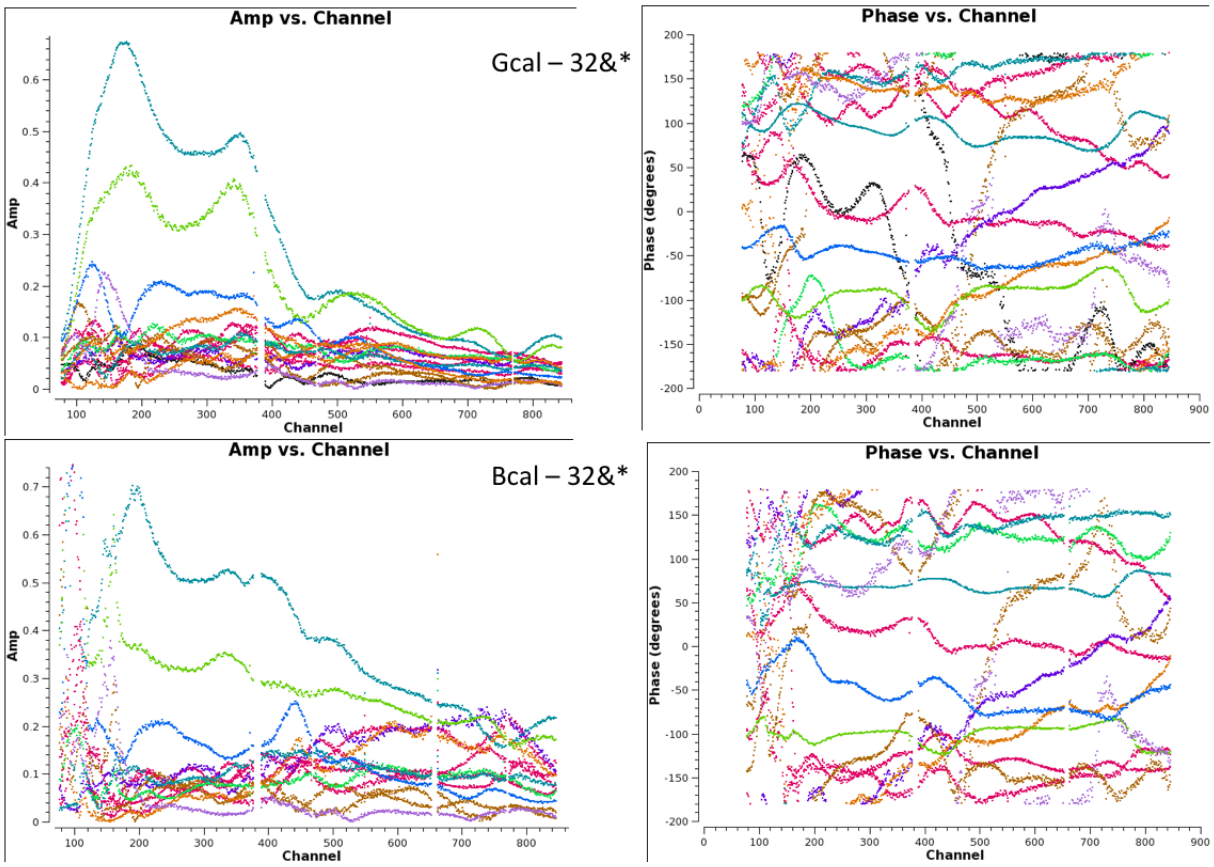

Fig. 5.— Upper: Visibility spectra (amplitude - left and phase - right), for all baselines to antenna 32, using the Galactic Center for calibration. Lower: Visibility spectra for all baselines to antenna 32, using the Bernardi sources for calibration.

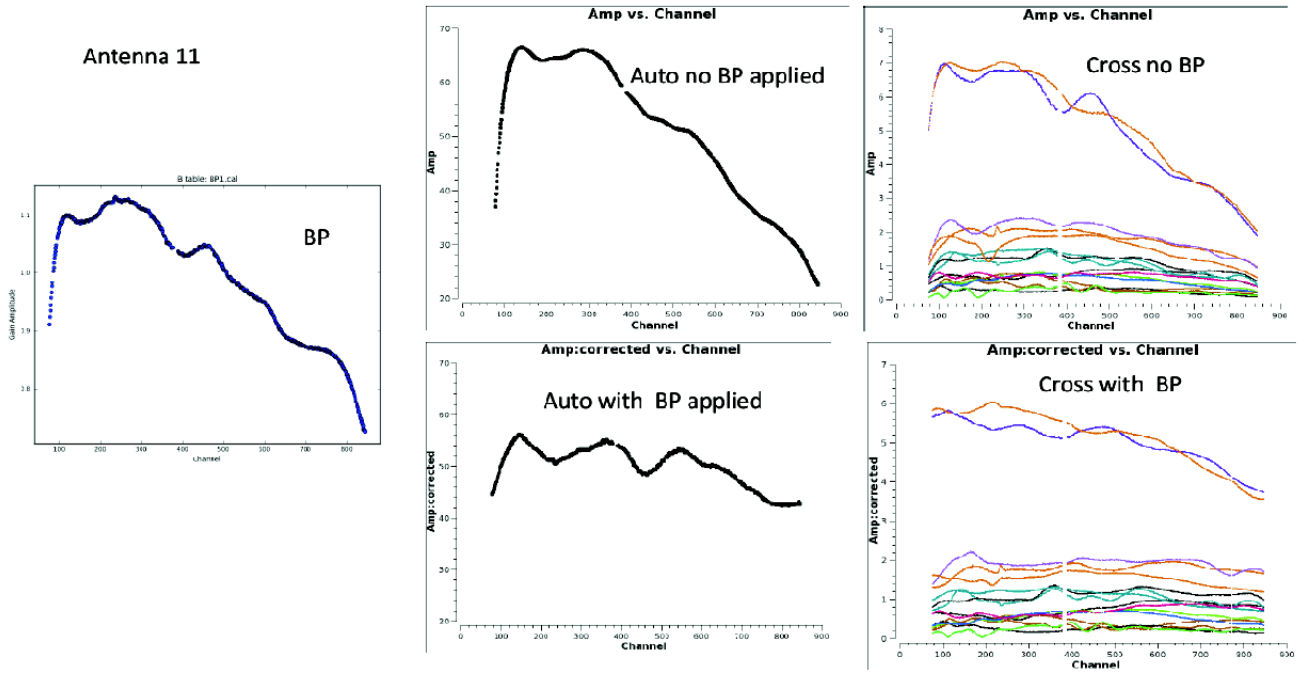

Fig. 6.— Data on the Galactic Center. Left: Bandpass solutions for Antenna 11 using the Galactic center for calibration. Center: Autocorrelations, calibrated and uncalibrated. Right: Cross correlations, calibrated and uncalibrated.

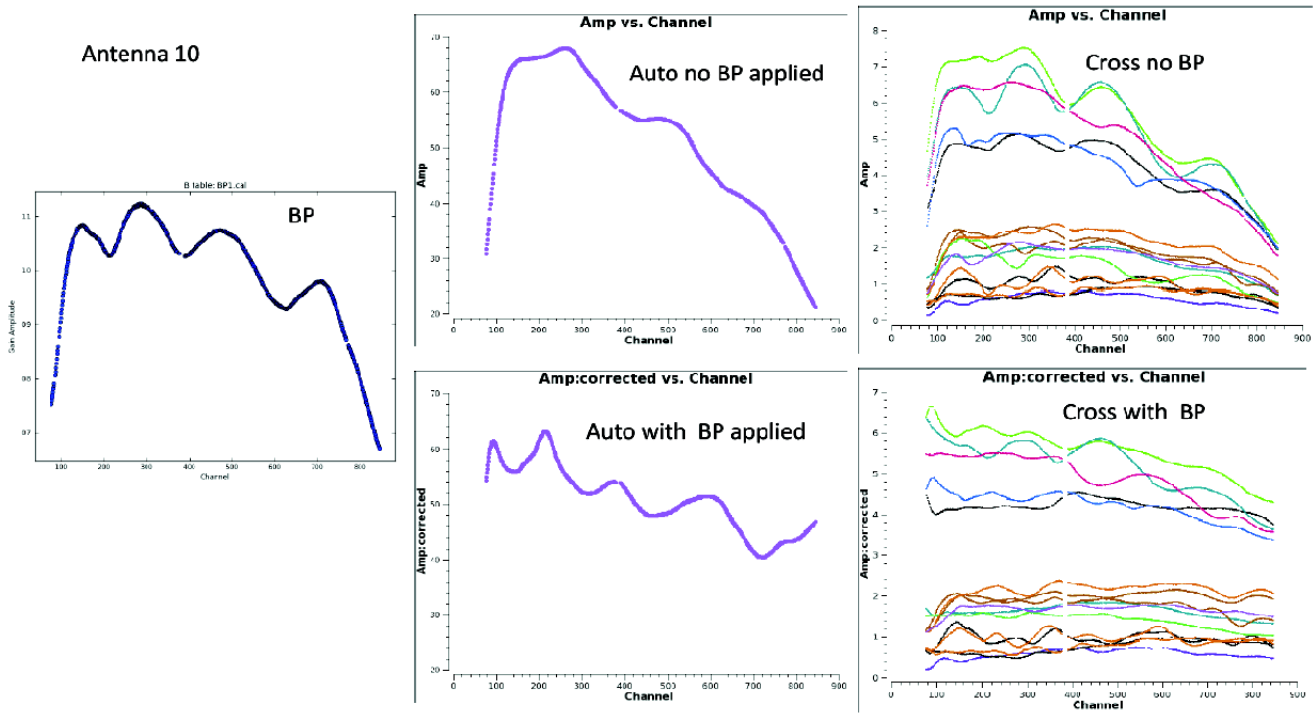

Fig. 7.— Data on the Galactic Center. Left: Bandpass solutions for Antenna 10 using the Galactic center for calibration. Center: Autocorrelations, calibrated and uncalibrated. Right: Cross correlations, calibrated and uncalibrated.

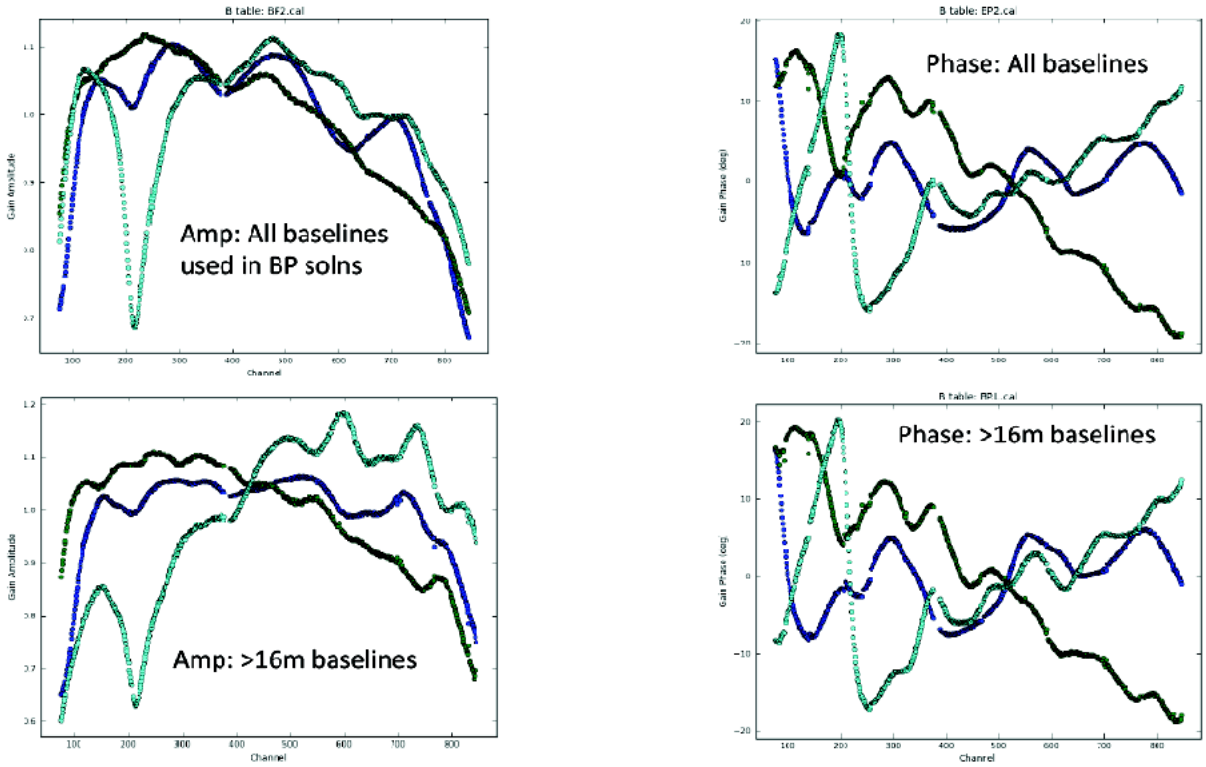

Fig. 8.— Upper: Bandpass solutions on the Galactic center for 3 antennas (10 = cyan, 11 = green, 73 = cyan), using all baselines in the array. Lower: same, but now omitting the shortest (15m) baselines in the bandpass calibration.

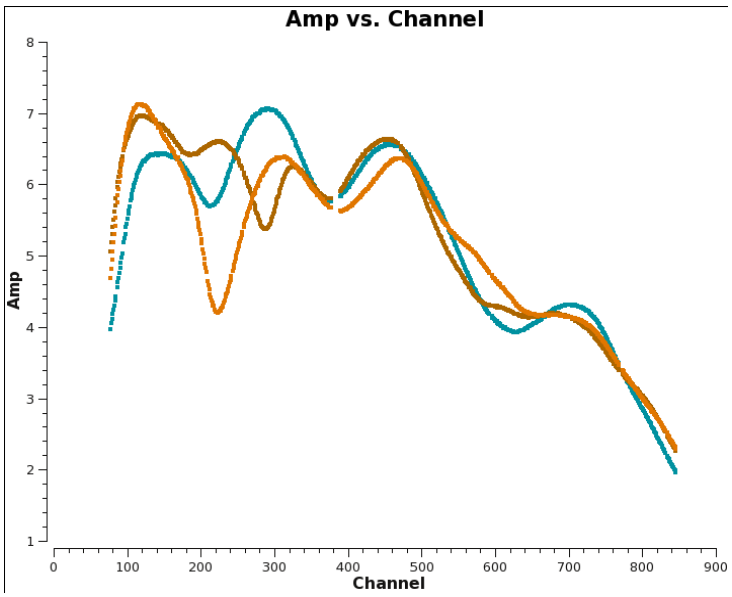

Fig. 9.— Uncalibrated visibility spectra for three 15m spacings oriented 45° from north (10-106 (cyan), 23-73 (orange), and 105-54 (brown)